Water Science & Technology

Water Science & Technology Vol 90 No 7, 2234 doi: 10.2166/wst.2024.318

Mathematical modeling of osmotic membrane bioreactor process for oily wastewater treatment

Hadeer Kadhim Mohammed[a], Ahmed Faiq Al-Alawy[b], Talib Rashid Abbas[c], Ali I. Al-Mosawi[b,*] and Miqat Hasan Salih[b]

[a] The National Nuclear, Radiological, Chemical and Biological Regulatory Authority, Council of Ministers, Baghdad, Iraq
[b] Department of Chemical Engineering, College of Engineering, University of Baghdad, Baghdad, Iraq
[c] Environment and Water Directorate, Ministry of Science and Technology, Baghdad, Iraq
*Corresponding author. E-mail: alialmosawi@coeng.uobaghdad.edu.iq

AIA, 0000-0002-8688-3208

ABSTRACT

To evaluate the disposal effluent from the Al-Daura refinery in Iraq, which comprises oily wastewater, a mathematical model has been developed for both forward osmosis (FO) and osmotic membrane bioreactor (OsMBR). The procedure is explained mathematically, accounting for both the concentration and polarization aspects. As a result of mathematical modeling, the water flux was determined by the osmotic pressure, the concentration, and the polarization of the feed and draw solutions. Based on traditional methods of predicting water flux using external and internal concentration polarizations, it is determined that water flux will occur in the first model (Model-1). To increase the accuracy of Model-1, the resistivity (K) of the solute has been modified to be independent of the diffusivity of the solute. The old model (Model-1) and the updated model (Model-2) overestimated water flux by 17 and 25%, respectively. It was possible to make a valid comparison between the experiment and theory based on the results of both experiments.

Key words: external concentration polarization, internal concentration polarization, modeling, wastewater, water flux

HIGHLIGHTS

- An osmotic membrane bioreactor (OsMBR) is an excellent choice for treating oily wastewater discharged from the Al-Daura refinery. The OsMBR process converts oily wastewater into high-quality water that can be reused in a variety of applications.
- Increasing the feed temperature, draw solution concentration, and feed flow rate increased the water flux from the forward osmosis process.

1. INTRODUCTION

The scarcity of fresh water is a fundamental issue in many parts of the world, and it affects many sectors of society. It has become increasingly evident in the 21st century that access to fresh water is one of the biggest obstacles, both in terms of consuming it and using it for other purposes (Al-Alawy & Salih 2016; Cairone *et al.* 2024; Guo *et al.* 2024). Globally, there are 2.2 billion people in the world who do not have access to clean water due to poor sanitation conditions. There is therefore no doubt that meeting the growing demands for clean water in the 21st century is going to be one of the greatest challenges of the century (Al-Alawy *et al.* 2017; Tortajada & Biswas 2018; United Nations 2023; Choque Campero *et al.*, 2024; WWAP 2024). As a general rule, wastewater is generated by two types of sources: industrial and human wastes. Industrial wastes come from companies such as oil refineries, where they generate industrial wastes. A refinery may discharge effluents that contain oil, grease, and hydrocarbons. These three contaminants are the most common ones that can be found in the effluents of refineries. Among the many biotreatment techniques that are currently being developed, there are membrane-based biotreatment technologies that show great promise, especially when it comes to the production of high-quality water that is free from contaminants and known to be unharmful to living organisms (Escobar 2010; Chung *et al.* 2012; Zhao *et al.* 2012; Im *et al.* 2021; Andrianov *et al.* 2023; Boubakri *et al.* 2024). Among the various ways to treat oily wastewater are solvent extractions, adsorptions, chemical oxidations, and biological treatments. Among the various ways of treating oily

wastewater are membrane bioreactors (MBRs), osmotic membrane bioreactors (OsMBRs), and conventional treatments. Regardless of whether the wastewater is organic or inorganic, the methods of treating it are the same. In terms of wastewater treatment processes, MBRs and OsMBRs stand out as the most effective ones. It is important to consider several factors when selecting the best water treatment strategy, such as water quality requirements, energy consumption, and operating costs (Al-Saffar & Al-Alawy 2002; Abass O *et al.* 2011; Abdul Wahab *et al.* 2015; Al-Asheh *et al.* 2021; Chang *et al.* 2022).

It has been noted that a variety of membrane separation techniques have been developed and are being applied for the treatment of industrial and municipal wastewaters in an attempt to make them drinkable. In order to achieve separation, there are two kinds of membranes that can be used. The first are those driven osmotically, such as forward osmosis (FO) membranes, and the second are those driven by pressure, such as nanofiltration, ultrafiltration, microfiltration, and reverse osmosis (RO) membranes. As the name implies, FO is a method of transporting water via natural osmosis from an aqueous solution through a membrane to an aqueous solution through a highly selective layer that has been created via nature (Ana Isabella Navarrete Pérez 2015; Mamah *et al.* 2022; Salamanca *et al.* 2023; Anh-Vu *et al.* 2024; Takabi *et al.* 2024). In contrast to pressure-driven membrane processes, FO is a naturally occurring, osmosis-driven process that involves a semi-permeable membrane. As an ideal barrier, the semi-permeable membrane allows water to pass while rejecting salts and other undesirable substances (Ma *et al.* 2013; Eyvaz *et al.* 2016; Iorhemen *et al.* 2016; Damirchi & Koyuncu 2021; Ozcan *et al.* 2023). An osmotic gradient is responsible for keeping the solute on both sides of a selectively permeable membrane when it transports water from the low-solute concentration feed solution (FS) to the concentrated draw solution (DS) (Al-Alawy *et al.* 2016; Damirchi & Koyuncu 2021; Kharraz *et al.* 2022; Han *et al.* 2023). In other words, FO deals with a physical phenomenon. FO processes utilize the osmotic pressure difference between feed and draw solutions to generate driving power. This result reduces energy costs and reduces membrane fouling, among other benefits. In addition to its low membrane fouling potential, the method operates with minimal hydraulic pressure and retains a wide variety of undesirable compounds (Holloway *et al.* 2007; Cornelissen *et al.* 2008; Kadhima *et al.* 2018; Schneider *et al.* 2021; Salih & Al-Alawy 2022a, 2022b; Chen *et al.* 2024; Liu *et al.* 2024).

2. MATHEMATICAL MODELING

2.1. Osmotic pressure

According to the relation of van't Hoff, the osmotic pressure (π) of a solution measured in bar units depends not only on the concentration of dissolved ions but also on the temperature of the solution (van't Hoff 1995; Alenezi & Merdaw 2021), as follows:

$$\pi = i\Phi MRT \tag{1}$$

where i represents the van̓ t Hoff factor (also known as dissociation factor), Φ is the osmotic coefficient, M is the molarity, R is the ideal gas constant (L bar/K mol), and T represents the absolute temperature (K). The van't Hoff factor is used to compensate deviations from ideality behavior of solutions where particles of a solute take a finite volume and are attracted to each other by van der Waals forces (Johnson *et al.* 2021). Generally, Φ depends on the solute type and concentration, where with a diluted concentration of the solute it will be equal to one. In the ideal solution, Φ is equal to one (Qasem *et al.* 2023). Table 1 illustrates values of osmotic coefficients and the van̓ t Hoff factor for a bunch of solutes with respect to physiological importance.

Table 1 | Osmotic coefficients and van't Hoff factors for a number of solutes (Khudair 2011; Bowden *et al.* 2012)

	Substance								
	NaCl	HCOONa	CH_3COONa	$CaCl_2$	$MgCl_2$	Na_2SO_4	$MgSO_4$	KCl	HCl
Φ	0.93	0.96	0.94	0.86	0.89	0.74	0.58	0.92	0.95
i	2	2	2	3	3	3	2	2	2

2.2. Modeling flux for osmotic process (Model-1)

Here's how FO, RO, and pressure-retarded osmosis (PRO) transport water (Cath *et al.* 2006):

$$J_w = A(\sigma\Delta\pi - \Delta P) \tag{2}$$

where J_w is water flux, A is the water permeability constant for the membrane, σ is the reflection coefficient, $\Delta\pi$ is the osmotic pressure difference, and ΔP is the hydraulic pressure, which is zero for FO, and with respect to RO, $\Delta P > \Delta\pi$, and for PRO, $\Delta\pi > \Delta P$ as shown in Figure 1.

The water flux, J_w, of the FO process is dependent on the flux over the selective layer of the membrane and is given as follows:

$$J_w = A(\pi_{d,w} - \pi_{f,w}) \tag{3}$$

where $\pi_{d,w} - \pi_{f,w}$ is the difference of the osmotic pressure through the FO membrane selective layer, which is also called effective pressure ($\Delta\pi_{eff}$). The osmotic reflection coefficient (σ) is assumed to be equal to one.

Concentration polarization (CP) is an important issue in water treatment with the usage of membrane technology and this problem has been investigated by many researchers. CP affects the permeate negatively via increasing osmotic pressure at the wall of the membrane active side. Usually, CP can take place on the membrane sides. At feed side, the solute will be concentrated on the membrane wall. While at the permeate side, the solute will be diluted at the membrane wall. These two phenomena are known as concentrative external concentration polarization (CECP) and dilutive external concentration polarization (DECP), respectively. In case of using an asymmetric membrane, one of these boundary layers take place inside the porous support layer of the membrane leading to protecting it from turbulence associated with cross flow as well as shear over the membrane surface. This state is referred to as either concentrative internal concentration polarization (CICP) or dilutive internal concentration polarization (DICP). In general, concentration polarization occurs in electrochemical systems when the bulk solution is significantly different from the electrode surface in terms of concentration. There can be a decrease in electrochemical reactions due to this difference. There are two types of this phenomenon, internal (ICP) and external concentration polarization (ECP). It is important to note that ICP occurs within the porous structure of an electrode, and ECP occurs at the interface between the electrode and the bulk solution (McCutcheon & Elimelech 2006; Tan & Ng 2008; Chae *et al.* 2024).

2.2.1. External concentration polarization

Concentrative ECP takes place in the FO process when the feed solution is cited toward the membrane active layer. It's important to know the overall effective osmotic driving force to account for the flux in FO. Therefore, it's necessary to calculate the concentration of the feed at the surface of the active layer. The surface concentration can be calculated

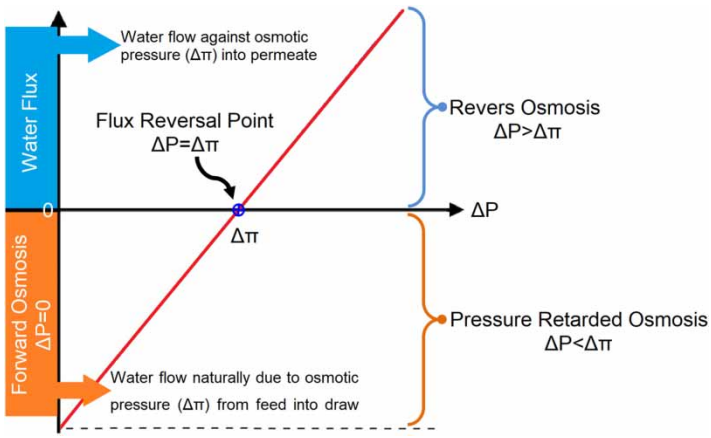

Figure 1 | Directions and values of water flux as a function of ΔP (Cath *et al.* 2006).

experimentally through utilizing boundary layer (BL) film theory (McCutcheon & Elimelech 2006). Based on the Sherwood number (Sh) determination in a rectangular channel, the following flow system can be formed:

For laminar flow:

$$\mathrm{Sh} = 1.85\left(\mathrm{Re}\,\mathrm{Sc}\frac{d_\mathrm{h}}{L}\right)^{0.33} \tag{4}$$

And for turbulent flow:

$$\mathrm{Sh} = 0.04\,\mathrm{Re}^{0.75}\mathrm{Sc}^{0.33} \tag{5}$$

where Re represents Reynolds number, Sc is Schmidt number, L is the channel length, and d_h is the hydraulic diameter. The relation describing hydraulic diameter for rectangular duct is

$$d_\mathrm{h} = \frac{2ab}{a+b} \tag{6}$$

where a and b are the dimensions of the duct. The coefficient of mass transfer, k, is associated with Sh to give

$$k = \frac{\mathrm{ShD}}{d_\mathrm{h}} \tag{7}$$

Here, D is the diffusivity of the solute. A mass balance can be presented at the membrane wall as follows:

$$\text{Accumulation of mass} = \text{inlet mass} - \text{outlet mass} \tag{8}$$

With steady state, no change of accumulation of mass and the flux of influent solute to the membrane surface should be equated by fluxes of effluent solute passing from the membrane (via diffusion) and across the membrane (into the permeate) as follows:

$$\frac{dM}{dt} = 0 = J_\mathrm{w}C\alpha - \frac{dC}{dx}Da - J_\mathrm{w}C_\mathrm{p}\alpha \tag{9}$$

where J_w is the water flux, M is the mass of solute, t is the time, x is the perpendicular distance to membrane wall, C is the solute concentration inside the BL, C_p is the concentration of the solute in the permeate side, and α is the membrane surface area. There is no limit to the application of Equation (9) at any plane in the BL and not only at the membrane surface, since the steady flow of solutes over the boundary layer prevents accumulation of solute within it. The last part in Equation (9) represents the solute that should transfer through the BL and the membrane to the permeate side. Rearranging and solving Equation (9) over the thickness of BL (δ) with the BL conditions: $C(0) = C_\mathrm{f,w}$ and $C(\delta) = C_\mathrm{f,b}$, where $C_\mathrm{f,b}$ is the bulk feed concentration and $C_\mathrm{f,w}$ is the concentration at the membrane wall, lead to the following equations:

$$D\int_{C_\mathrm{f,w}}^{C_\mathrm{f,b}}\frac{dC}{C - C_\mathrm{p}} = -J_\mathrm{w}\int_0^\delta dx \tag{10}$$

Equation (10) can be integrated to give (assuming concentration of solute in permeate is zero)

$$\ln\frac{C_\mathrm{f,w}}{C_\mathrm{f,b}} = J_\mathrm{w}\delta/D = J_\mathrm{w}/k \tag{11}$$

where δ is the thickness of the BL. Rearranging Equation (11) using the van't Hoff relation gives the model of the CECP for

each of the permeate fluxes. The mass transfer coefficient is utilized to determine the CECP mode, as follows:

$$\frac{\pi_{f,w}}{\pi_{f,b}} = \exp(J_w/k) \tag{12}$$

where J_w is the water permeate, and $\pi_{f,w}$ and $\pi_{f,b}$ are the feed solution osmotic pressures at the membrane wall and the bulk, respectively. The positive sign of the exponent indicates that $\pi_{f,w} > \pi_{f,b}$. CECP take place solely at the membrane feed side. Besides, it's assumed in this relation that the ratio of feed solute concentration to the bulk concentration at the membrane wall balances the ratios of osmotic pressures. This is acceptable hypothesis for diluted solutions where osmotic pressure is related to salt concentration.

A diluted ECP has a lower membrane wall concentration than the bulk solute, as indicated by the following equation. This state decreases the draw solution's effective driving force. Dilutive ECP characterized with that the concentration of membrane wall of the draw solute is less than that of the bulk (Tang *et al.* 2010):

$$\frac{\pi_{d,w}}{\pi_{d,b}} = \exp\left(-\frac{J_w}{k}\right) \tag{13}$$

Here, $\pi_{d,w}$ and $\pi_{d,b}$ are the draw solution osmotic pressures at the membrane wall and at the bulk, respectively. It is assumed, as revealed in Equation (13), that the ratio of the draw solute concentration of the membrane wall to the concentration of bulk balances the ratio of osmotic pressures at the same side. To represent the FO process flux in the existence of ECP, we begin with the general FO equation of flux, given as follows:

$$J_w = A(\pi_{d,b} - \pi_{f,b}) \tag{14}$$

where A is the permeability coefficient of pure water. The coefficient of osmotic reflection (σ) is assumed to have a magnitude of 1, because no reverse salt transfer occurs across the membrane. Equation (14) predicts flux that is proportional to driving force without the presence of CECP or DECP, which might be valid when the permeate rate is very low. When permeate flux becomes relatively high, this equation must be modified for both the CECP and DECP to be included:

$$J_w = A\left[\pi_{d,b}\exp\left(-\frac{J_w}{k}\right) - \pi_{f,b}\exp\left(\frac{J_w}{k}\right)\right] \tag{15}$$

The utilization of this flux model is limited because the dense symmetric membranes for osmotic processes are unused. Due to this, it must take into account the state where the membrane is asymmetric, making ICP effects the most important.

2.2.2. Internal concentration polarization

Using the convection–diffusion relation, Lee *et al.* (1981) developed a model for the determination of the CICP layer in PRO mode. The simplified model, however, was applicable for low water fluxes. Loeb *et al.* (1997) utilized the upcoming relation for DICP (FO mode) and CICP, respectively, which was used by McCutcheon & Elimelech (2006) to describe the FO process.

$$K = \left(\frac{1}{J_w}\right)\ln\frac{B + A\pi_{d,w} - J_w}{B + A\pi_{f,b}} \tag{16}$$

where K is the solute resistivity for diffusion within the porous support layer, which is given as

$$K = \frac{t\tau}{D\varepsilon} = \frac{S}{D} \tag{17}$$

where S is the membrane structural parameter, t is membrane thickness, ε is the porosity of the support layer, τ is the tortuosity of the membrane, and D is the solute diffusion coefficient. In this equation, K is dependent on diffusivity. B in Equation

(16) is the salt permeability coefficient within active layer of the membrane, which can be calculated using the following relation:

$$B = \frac{(1 - R) * J_w}{R} \tag{18}$$

where R is the solute rejection, which is related to the membrane characteristic. Salt permeability coefficient (B) is nearly negligible when compared with the other terms in Equation (16). Thus, salt flux in the direction of water flux is ignored as well as any movement of salt from the permeate (draw solution) side to the feed side (Gray *et al.* 2006). Therefore, Equation (16) can be simplified for water flux as follows:

$$J_w = A[\pi_{d,w} - \pi_{f,b} \exp(J_w K)] \tag{19}$$

The exponential term in Equation (19) represents the correction factor, which can be considered as the CECP modulus and defined as

$$\frac{\pi_{f,i}}{\pi_{f,b}} = \exp(J_w K) \tag{20}$$

where $\pi_{f,i}$ is the osmotic pressure of the feed inside the active layer. The positive sign of the exponent denotes that $\pi_{f,i} > \pi_{f,b}$, which indicates concentrative influence. Substitute Equation (12) into Equation (19) to get an analytical relation that gathers the influence of ICP and ECP on water flux, as follows:

$$J_w = A[\pi_{d,b} \exp(-J_w/k) - \pi_{f,b} \exp(J_w K)] \tag{21}$$

All the elements in Equation (21) can be determined analytically or by experiments. Therefore, water flux can be determined for the PRO mode as shown in Figure 2.

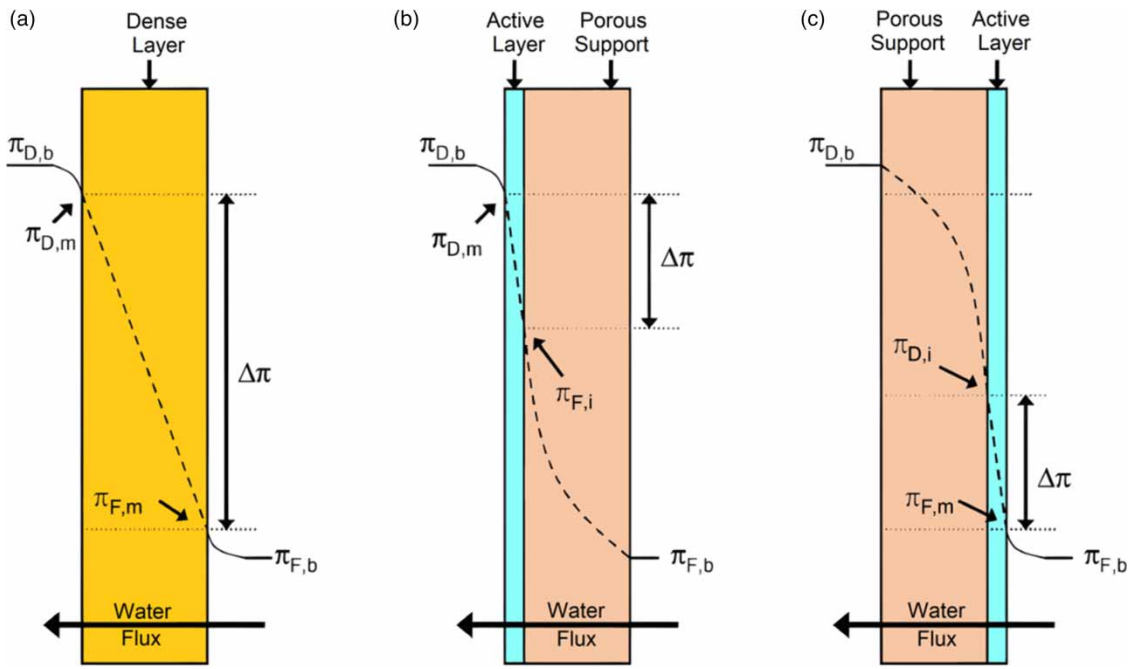

Figure 2 | Specify ICP and ECP profiles for osmotic driving forces. (a) A plot depicting concentrative and dilutive external CP. (b) The plot shows a concentration of internal CP and a dilution of external CP (PRO mode). (c) The plot displays dilutive and concentrated internal concentrations of CO (FO mode) (McCutcheon & Elimelech 2006).

The dilutive ICP state is characterized for FO, where the membrane active layer is located against the feed side and the porous support layer is against the draw side (Kessler & Moody 1976). When water penetrates the active layer, the draw solution inside the porous structure is diluted. This is called dilutive ICP (Figure 2). Loeb *et al.* (1997) described this phenomenon for FO as follows:

$$K = \left(\frac{1}{J_w}\right) \ln \frac{B + A\pi_{d,b}}{B + J_w + A\pi_{f,w}} \tag{22}$$

When considering that the salt permeability (B) is neglected. Equation (22) can be rearranged to get the following water flux equation:

$$J_w = A[\pi_{d.b} \exp(-J_w K) - \pi_{f,w}] \tag{23}$$

Here $\pi_{d,b}$ is now modified by the DICP modulus, given by

$$\frac{\pi_{d,i}}{\pi_{d,b}} = \exp(-J_w K) \tag{24}$$

where $\pi_{d,i}$ represents the draw solution concentration inside the active layer. The negative sign refers to the direction of water flux, which is away from the membrane active layer, which means the CP effect is dilutive, i.e. $\pi_{d,i} < \pi_{d,b}$ by substituting Equation (12) into Equation (23), we get

$$J_w = A[\pi_{d,b} \exp(-J_w K) - \pi_{f,b} \exp(J_w/K)] \tag{25}$$

The parameters in Equation (25) are system conditions and membrane parameters that are measurable. The iteration steps required to obtain water flux using Model-1 for FO mode are shown in Figure 3. In this relation, DICP is combined with CECP. Operating conditions and concentrations of feed and draw solutions are given.

2.3. Modified model for ICP layer (Model-2)

Model-2 focuses on developing the correlations between solute resistivity coefficients (K) and their relations hips with diffusivity, while the equations used in Model-1 that relate mass transfer coefficients (film model) are used in Model-2 as well. There is a possibility that the constant solute resistance coefficient (K) may not be true, as it is attributed to the fact that the diffusivity coefficient may not be constant, especially in the case of a large concentration difference between the solute and the membrane. In order to analyze the influence of K on water flux, modeling by using a constant value of K would be under-researched. A relation for ICP layer modeling has been developed by Loeb *et al.* (1997), which has been modified from the governed equations used in this study. The solute flux, J_s, over the dense layer for DICP is given as

$$-J_s = B(C_{d,w} - C_{f,w}) \tag{26}$$

The flux of the solute over the porous layer of the FO membrane can be written using the equation of convection and diffusion as follows:

$$-J_s = \varepsilon \frac{dD_{C(x)}C(x)}{dx} - J_w C(x) \tag{27}$$

The solute diffusion coefficient can be represented as a function of the solute concentration over Distance x as follows:

$$D_{C(x)} = E_1 + E_2 C_x + E_3 C_x^2 + \cdots + E_n C_x^{n-1} \tag{28}$$

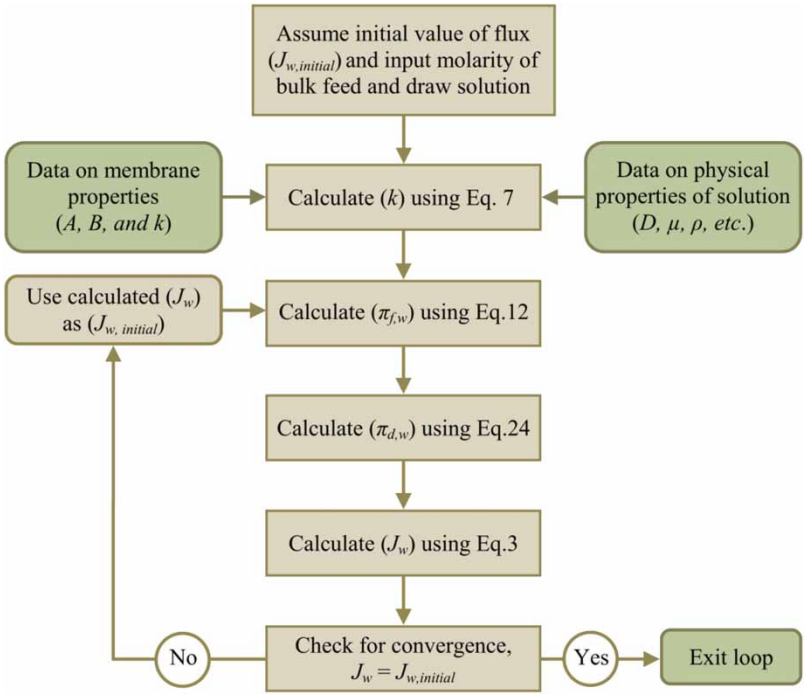

Figure 3 | Iteration process using software solved mathematically for water flux, J_w, (using Model-1) for FO mode.

The term x is the vertical distance from the membrane selective layer that is determined inside the porous support layer and the coefficients E_i represent constants accompanied by the mathematical relation of diffusion coefficient and their values depend on the type of salt used. The E_i values for NaCl salt are listed in Table 2.

Combining Equations (26) and (27) yields

$$B(C_{d,w} - C_{f,w}) = \varepsilon \frac{dD_{C(x)}C(x)}{dx} - J_w C(x) \tag{29}$$

The relevant boundary conditions are defined in Figure 2 for the FO mode and represented as

$$C(x) = C_{d,w} \text{ at } x = 0 \text{ and } C(x) = C_{d,b} \text{ at } x = t$$

By applying the boundary conditions, Equation (29), which is a separable differential equation, can be solved by MATLAB software for dilutive ICP (FO mode) to give (Tan & Ng 2013; Majid *et al.* 2023; Chong *et al.* 2024) the following:

$$K^* = \left[\frac{F_1}{J_w}(C_{d,b} - C_{d,w}) + \frac{F_2}{J_w}\left(C_{d,b}^2 - C_{d,w}^2 + \frac{F_n}{J_w}\left(C_{d,b}^n - C_{d,w}^n\right)\right)\right] + \frac{G}{J_w}\ln\left(\frac{B(C_{d,w} - C_{f,w}) + J_w C_{d,b}}{B(C_{d,w} - C_{f,w}) + J_w C_{d,w}}\right) \tag{30}$$

Table 2 | E_i values for NaCl salt

E_i	E_1	E_2	E_3	E_4
Value	$14{,}900 \times 10^{-13}$	-398×10^{-13}	418×10^{-13}	-77.6×10^{-13}

In a similar manner, the relation for CICP (PRO mode) for the FO process can also be modified and written as

$$K^* = \left[\frac{F_1}{J_w}(C_{d,w} - C_{d,b}) + \frac{F_2}{J_w}\left(C_{d,w}^2 - C_{d,b}^2\right) + \frac{F_n}{J_w}\left(C_{d,w}^n - C_{d,b}^n\right)\right] + \frac{G}{J_w}\ln\left(\frac{B(C_{f,w} - C_{d,w}) + J_w C_{d,w}}{B(C_{f,w} - C_{d,w}) + J_w C_{d,b}}\right) \quad (31)$$

When solving Equation (29), with respect to NaCl as a draw salt, Equations (30) and (31) become, respectively:

$$K^* = \left[\frac{6.67 \times 10^{-12}}{J_w}(C_{d,b} - C_{d,w}) + \frac{-1.33 \times 10^{-10}}{J_w}(C_{d,b}^2 - C_{d,w}^2) + \frac{-5.40 \times 10^{-8}}{J_w}(C_{d,b}^3 - C_{d,w}^3)\right] + \frac{1.71 \times 10^{-9}}{J_w}\ln\left(\frac{B(C_{d,w} - C_{f,w}) + J_w C_{d,b}}{B(C_{d,w} - C_{f,w}) + J_w C_{d,w}}\right) \quad (32)$$

$$K^* = \left[\frac{6.67 \times 10^{-12}}{J_w}(C_{d,w} - C_{d,b}) + \frac{-1.33 \times 10^{-10}}{J_w}(C_{d,w}^2 - C_{d,b}^2) + \frac{-5.40 \times 10^{-8}}{J_w}(C_{d,w}^3 - C_{d,b}^3)\right] + \frac{1.71 \times 10^{-9}}{J_w}\ln\left(\frac{B(C_{f,w} - C_{d,w}) + J_w C_{d,w}}{B(C_{f,w} - C_{d,w}) + J_w C_{d,b}}\right) \quad (33)$$

The modified solute resistivity (K^*) will be written as

$$K* = t\tau/\varepsilon \quad (34)$$

The solute resistivity (K^*) used in this study has to be calculated for the FO membrane with respect to membrane structure and it is constant for each membrane and not influenced by other conditions of the process. The iteration steps required to obtain water flux using Model-2 for FO mode are shown in Figure 4. The operating conditions and concentrations of feed and draw solutions are given.

2.4. Recovery percentage

The recovery refers to the quantity of feed that's recovered as permeate and it is written as a percentage (Kessler & Moody 1976). The membrane recovery was calculated by dividing the permeate volume (V_p) by the feed volume (V_f). The recovery is defined as

$$\text{Recovery}\,\% = (V_p/V_f) \times 100 \quad (35)$$

3. RESULTS AND DISCUSSION

3.1. Mathematical modeling of flux behavior in FO process and biological process

Three types of membranes, cellulose triacetate (CTA), cellulose acetate (CA), and thin-film composite (TFC), have been selected based on previous studies and practical experience in this field. Several studies have demonstrated that CTA and CA membranes are efficient for FO, as well as being cost-effective. The TFC membrane is widely used in RO, and was compared with CTA and CA membranes in this study. The FO water flux was calculated theoretically using Equation (14) without consideration of concentration polarization or fouling influences. Moreover, two models were used in this study, the conventional model referred to as Model-1 and the modified model referred to as Model-2. There are a number of factors that affect the equations used for determining water flux in the two models, including the temperature of the feed and draw solutions, their concentrations, their flow rates, the solute diffusion coefficient, permeability coefficient, mass transfer coefficient, the solute resistance, modified solute resistance, membrane thickness, tortuosity, and porosity.

Figure 5 represents the relation between pure water flux vs. applied pressure for TFC, CA, and CTA membranes, and Table 3 represents the results of water permeability for these three membranes, respectively. From the figure and table, we can see that the permeability of TFC and CA membranes is much superior to that of the CTA membrane, where the value of the TFC membrane was nine times greater than that of the CA membrane, and one and a half times greater than that of the CA membrane. These results prove that TFC and CA RO membranes give high fluxes under hydraulic pressure.

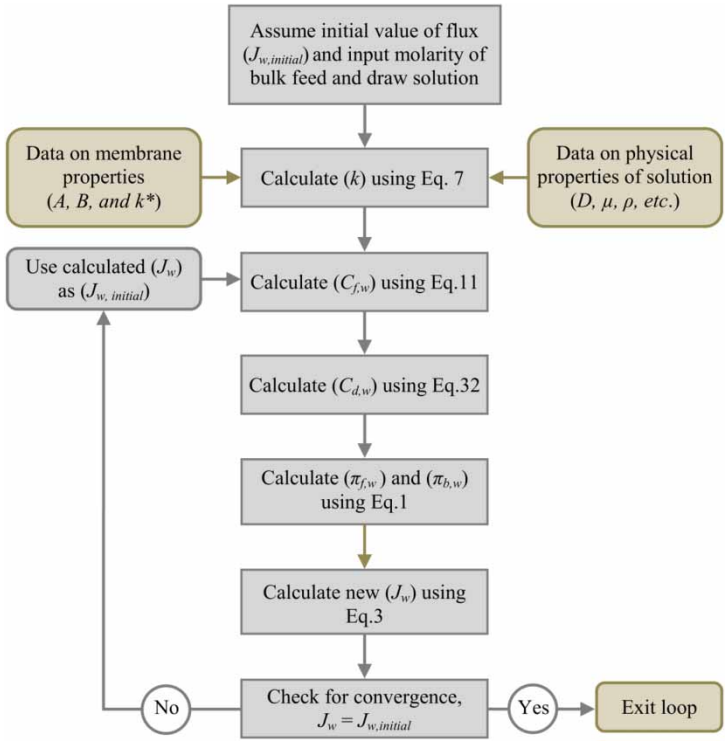

Figure 4 | Iteration process using software solved mathematically for water flux, J_w, (using Model-2) for FO mode.

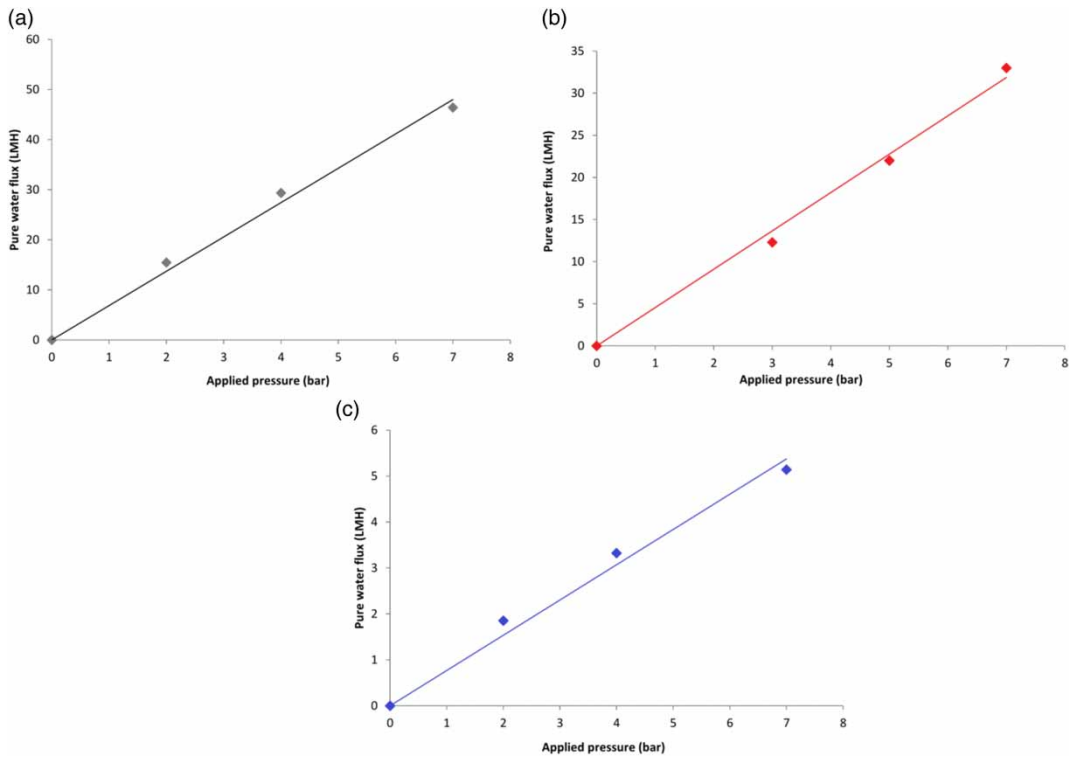

Figure 5 | Pure water flux against applied pressure for (a) TFC, (b) CA, and (c) CTA membranes at 30 °C.

Table 3 | Water permeability of TFC, CA, and CTA membranes

Membrane	TFC	CA	CTA
Water permeability, slope y	6.606x	4.69x	0.727x
Correlation factor, R^2	0.9921	0.9937	0.9849

Figure 6 illustrates the theoretical and experimental effects of concentration on water flux for the three draw solutions, sodium chloride, sodium formate, and sodium acetate, as well as the models that are applied to each draw solution. Based on the flux data, the three draw solutions perform approximately the same for each model, demonstrating that the modified model, which represents ICP development, is more predictive and realistic than the traditional model (Model-1). The conventional model (model-1) over-predicted the water flux by more than 25% while the modified model (Model-2) over-predicted the water flux by 17%.

Figure 7(a) shows the theoretical and experimental water flux for an abiotic process done on CTA membranes. Therefore, it is evident that both models exhibit approximately the same response to changes in feed flow rate, based on the comparison between them. Figure 7(b) and 7(c) shows the deviation of the theoretical models from the experimental results for CA and TFC membranes, respectively. The same response was observed that Model-2 is more predictive than Model-1, proving the modifications carried out on ICP were satisfied.

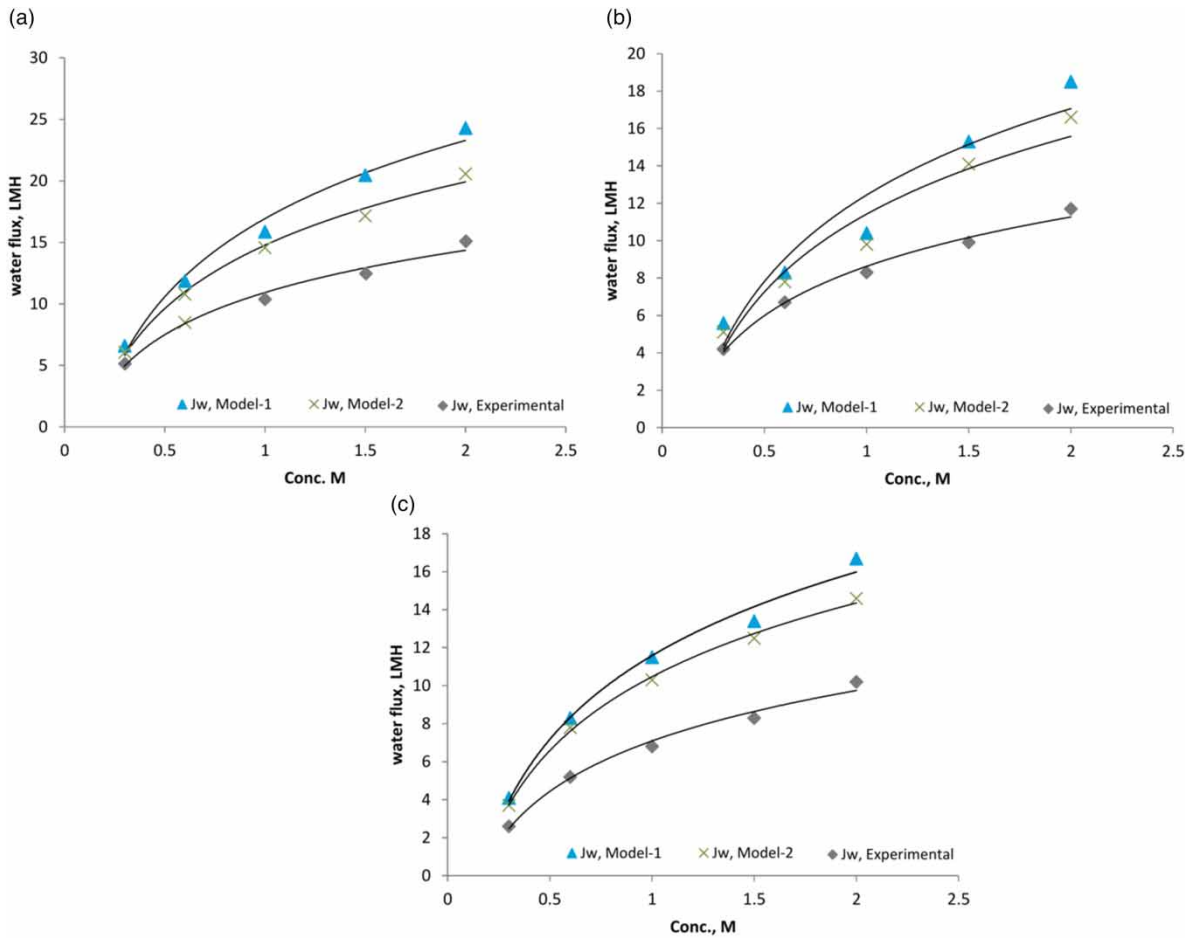

Figure 6 | Theoretical and experimental water flux for abiotic processes using (a) sodium chloride, (b) sodium formate, and (c) sodium acetate ($T = 30$ °C, $Q_{FS} = Q_{DS} = 3$ l/min, CTA membrane).

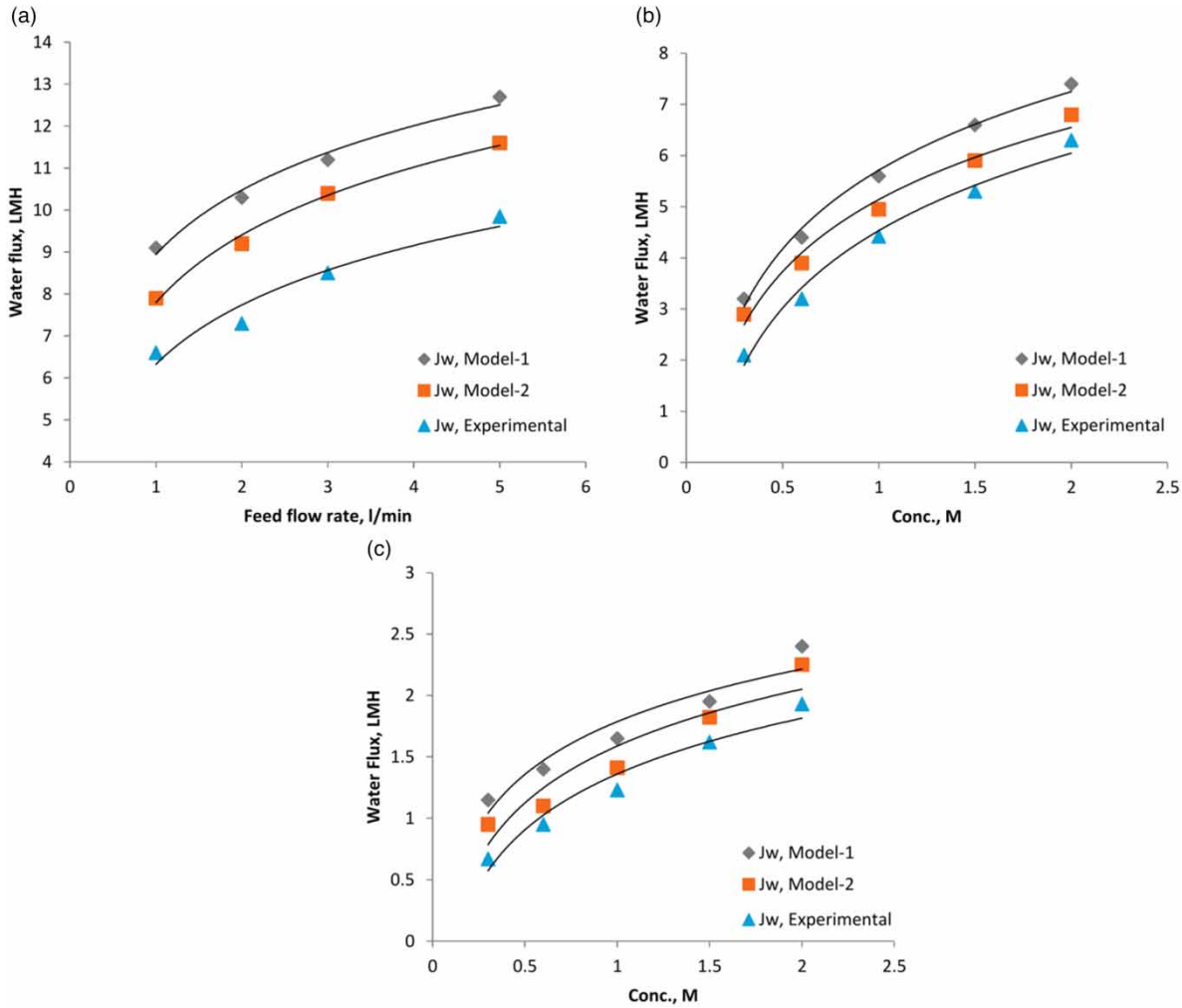

Figure 7 | Theoretical and experimental water flux for abiotic processes, (a) CTA, (b) CA, and (c) TFC membrane ($T = 30$ °C, $Q_{FS} = Q_{DS} = 3$ l/min, 0.6 M NaCl).

Figure 8 illustrates the relationship between the mass transfer coefficient and the feed flow rate of a CTA membrane. According to this figure, we can see an increase in the mass transfer coefficient (k) for CTA membranes as a function of the flow rate. Based on the following mathematical equation, we know that the mass coefficient is directly proportional to the velocity through its direct relationship with Sherwood's number, which can be expressed as follows:

$$\mathrm{Sh} = KL/Dc \tag{36}$$

Furthermore, it is directly proportional to the Reynolds number, which is used in order to measure the flow speed. As a result of the experiments (Al-Alawy *et al.* 2016), it has been demonstrated that the feed flow rate increases with an increase in water flux. Accordingly, as the flow rate increases, the mass transfer coefficient increases, as does the water flux, both of which increase simultaneously as the flow rate increases.

An illustration of a continuous biological process is shown in Figure 9(a) and 9(b), where the two models have been applied to a single CTA membrane in both side-stream and submerged modes, respectively, for the purpose of illustrating a biological continuous process. Due to the modification of the model (Equation (32)), it has been found that the water flux has been over-predicted by approximately 37%, while the traditional model (Equation (12)) has overpredicted by nearly 60%, therefore the change in the model has yielded a significantly higher prediction. The efficiency of the side-stream mode is better than the submerged mode in terms of productivity when comparing their obtained results with the practical results.

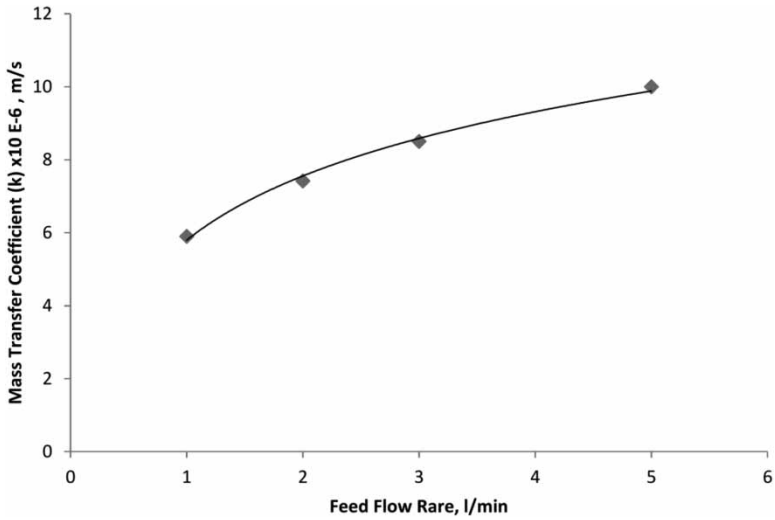

Figure 8 | Mass transfer coefficient vs. feed flow rate for CTA membrane ($T = 30$ °C, $Q_{DS} = 3$ l/min, 0.6 M NaCl).

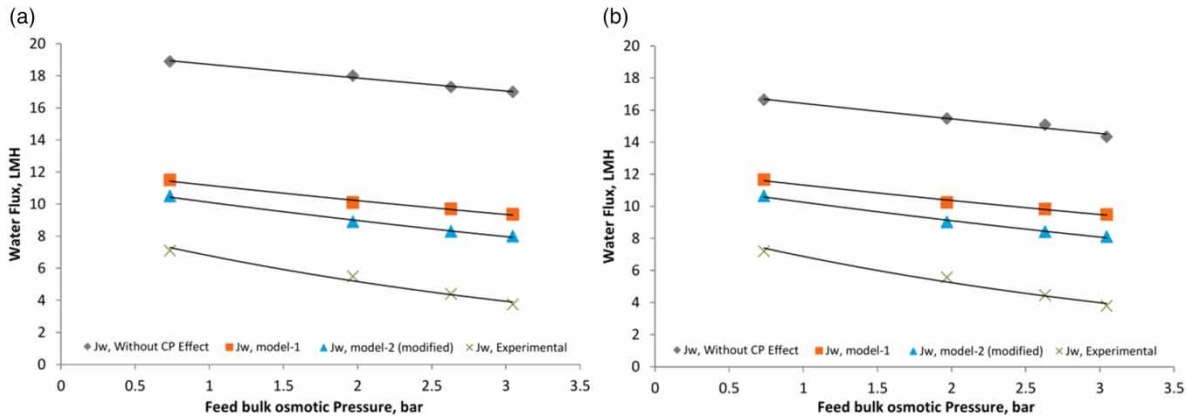

Figure 9 | Theoretical and experimental water flux for biological processes (a) side-stream mode and (b) submerged mode ($T = 30$ °C, $Q_{FS} = Q_{DS} = 3$ l/min).

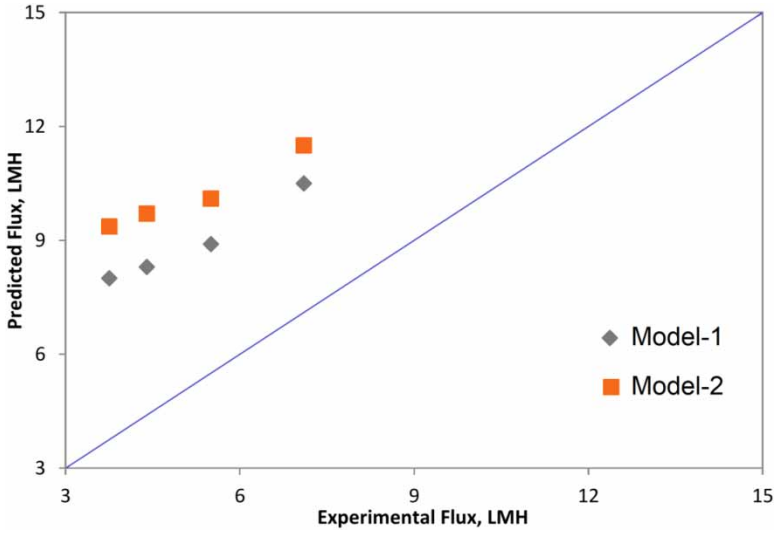

Figure 10 | Deviation of predicted flux for Model-1 and Model-2 from experimental flux for the side-stream mode.

Table 4 | Statistical analysis of the models for the side-stream mode

Parameter	Model-1	Model-2
Correlation factor, R^2	0.9635	0.970
Variance	0.6626	0.93125
Standard of deviation	0.814	0.965
Confidence level	95%	95%
No. of observation	4	4

Based on the investigation, the large deviation in forecasted water flow was attributed to fouling parameters that were affected, resulting in a decline in water flow. With respect to the modified model, the diffusivity coefficient equation (Equation (28)) is incorporated into the integration term and yields K^*, which is independent of the diffusivity coefficient. According to Figure 10 and Table 4, this will improve the accuracy of the prediction of water flux in the FO process.

4. CONCLUSIONS

1. OsMBRs are an effective means of treating oily wastewater discharged from Al-Daura refineries. With OsMBR, high-quality water can be produced from oily wastewater, which can be reused in a wide range of applications.
2. CTA membranes have a higher flux permeability than TFC and CA membranes. Consequently, CTA membranes produced two times more water flux than CA membranes and six times more than TFC membranes. These membranes were arranged according to the water flux order, including CTA, CA, and TFC. In comparison to CA and TFC membranes, CTA membranes have a higher reverse salt flux.
3. In response to higher feed temperatures, higher draw solution concentrations, and higher feed flow rates, a greater amount of water was reclaimed through FO. An increase in run time and draw flow rate is accompanied by a decrease in water flux.
4. When the concentration of the draw solution increases over time, reverse salt flux decreases.
5. There was approximately a 25% difference between the numerical model (Model-1) and the experimental value of water flux. Compared with the experimental results, the updated model (Model-2) showed a deviation of almost 17%, indicating a more realistic estimate.
6. In both methods, side-stream and submerged, the withdrawal solution flow rate and experiment time increase, resulting in a decrease in water flux. However, the side-stream mode produced the best productivity results. In the same way, reverse salt flux is also applicable.

DATA AVAILABILITY STATEMENT

All relevant data are available on request from the authors.

CONFLICT OF INTEREST

The authors declare there is no conflict.

REFERENCES

Abass, O. A., Jameel, A. T., Muyubi, S. A., Abdul Karim, M. I. & Alam, M. Z. (2011) Removal of oil and grease as emerging pollutants of concern (EPC) in wastewater stream, *IIUM Engineering Journal* **12** (4), 161–169. https://doi.org/10.31436/iiumej.v12i4.218.

Abdul Wahab, M. I., Saleh, H. I. & Al-Alawy, A. F. (2015) Performance of manipulated direct osmosis in water desalination process, *International Journal of Science and Technology*, **4** (10), 458–468.

Al-Alawy, A. F. & Salih, M. H. (2016) Experimental study and mathematical modelling of zinc removal by reverse osmosis membranes, *Iraqi Journal of Chemical and Petroleum Engineering*, **17** (3), 57–73. https://doi.org/10.31699/IJCPE.2016.3.5.

Al-Alawy, A. F., Abbas, T. R. & Mohammed, H. K. (2016) Osmotic membrane bioreactor for oily wastewater treatment using external & internal configurations, *Iraqi Journal of Chemical and Petroleum Engineering*, **17** (4), 71–82. https://doi.org/10.31699/IJCPE.2016.4.7.

Al-Alawy, A. F., Abbas, T. R. & Mohammed, H. K. (2017) Comparative study for organic and inorganic draw solutions in forward osmosis, *Al-Khwarizmi Engineering Journal*, **13** (1), 94–102. https://doi.org/10.22153/kej.2017.08.007.

Al-Asheh, S., Bagheri, M. & Aidan, A. (2021) Membrane bioreactor for wastewater treatment: A review, *Case Studies in Chemical and Environmental Engineering*, **4**, 100109. https://doi.org/10.1016/j.cscee.2021.100109.

Alenezi, I. A. & Merdaw, A. A. (2021) Proportionality of solute flux and permeability to water flux and permeability in forward osmosis process, *Desalination and Water Treatment*, **225**, 29–36. https://doi.org/10.5004/dwt.2021.27210.

Al-Saffar, T. A. & Al-Alawy, A. F. (2002) Study of the factors affecting the efficiency of reverse osmosis process, *Iraqi Journal of Chemical and Petroleum Engineering*, **3** (1), 49–55. https://doi.org/10.31699/IJCPE.2002.1.9.

Ana Isabella Navarrete Pérez (2015) *Analysis and Improvement Proposal of a Wastewater Treatment Plant in a Mexican Refinery. MSc Thesis*, Chalmers University of Technology, Gothenburg, Sweden. publications.lib.chalmers.se/records/fulltext/222932/222932.pdf.

Andrianov, A. P., Yantsen, O. V. & Efremov, R. V. (2023) State-of-the-art of forward osmosis technology: Prospects and limitations, *Membranes and Membrane Technologies*, **5** (4), 276–289. https://doi.org/10.1134/S2517751623040029.

Anh-Vu, N., Nomura, Y., Hidaka, T. & Fujiwara, T. (2024) Forward osmosis membrane process: A review of temperature effects on system performance and membrane parameters from experimental studies, *Journal of Environmental Chemical Engineering*, **12** (5), 113429. https://doi.org/10.1016/j.jece.2024.113429.

Boubakri, A., Elgharbi, S., Bouguecha, S., Bechambi, O., Bilel, H., Alanazy, H. D. & Hafiane, A. (2024) Accurate prediction of reverse solute flux in forward osmosis systems using comparative machine learning models, *Arabian Journal for Science and Engineering*, 2024. https://doi.org/10.1007/s13369-024-09267-0.

Bowden, K. S., Achilli, A. & Childress, A. E. (2012) Organic ionic salt draw solutions for osmotic membrane bioreactors, *Bioresource Technology*, **122**, 207–216. https://doi.org/10.1016/j.biortech.2012.06.026.

Cairone, S., Hasan, S. W. & Choo, K.-H., Li, C.-W., Zarra, T., Belgiorno, V. & Naddeo, V. (2024) Integrating artificial intelligence modeling and membrane technologies for advanced wastewater treatment: Research progress and future perspectives, *Science of The Total Environment*, **944**, 173999. https://doi.org/10.1016/j.scitotenv.2024.173999.

Cath, T. Y., Childress, A. E. & Elimelech, M. (2006) Forward osmosis: Principles, applications, and recent developments, *Journal of Membrane Science*, **281** (1–2), 70–87. https://doi.org/10.1016/j.memsci.2006.05.048.

Chae, S. H., Rho, H. & Moon, S. (2024) Modeling study of the effects of intrinsic membrane parameters on dilutive external concentration polarization occurring during forward and pressure-retarded osmosis, *Desalination*, **569**, 117043. https://doi.org/10.1016/j.desal.2023.117043.

Chang, H.-M., Xu, Y., Chen, S.-S. & He, Z. (2022) Enhanced understanding of osmotic membrane bioreactors through machine learning modeling of water flux and salinity, *Science of The Total Environment*, **838** (Part 1), 156009. https://doi.org/10.1016/j.scitotenv.2022.156009.

Chen, M., Heijman, S. G. J. & Rietveld, L. C. (2024) Ceramic membrane filtration for oily wastewater treatment: Basics, membrane fouling and fouling control, *Desalination*, **583**, 117727. https://doi.org/10.1016/j.desal.2024.117727.

Chong, Y. K., Fletcher, D. F. & Liang, Y. Y. (2024) CFD simulation of hydrodynamics and concentration polarization in osmotically assisted reverse osmosis membrane systems, *Journal of Water Process Engineering*, **57**, 104535. https://doi.org/10.1016/j.jwpe.2023.104535.

Choque Campero, L. A., Wang, W., Cardozo, E. & Martin, A. (2024) Decentralized biomass-based Brayton-Stirling power cycle with an air gap membrane distiller for supplying electricity, heat and clean water in rural areas, *Applied Thermal Engineering*, **254**, 123889. https://doi.org/10.1016/j.applthermaleng.2024.123889.

Chung, T.-S., Li, X., Ong, R. C., Ge, Q., Wang, H. & Han, G. (2012) Emerging forward osmosis (FO) technologies and challenges ahead for clean water and clean energy applications, *Current Opinion in Chemical Engineering*, **1** (3), 246–257. https://doi.org/10.1016/j.coche.2012.07.004.

Cornelissen, E. R., Harmsen, D., de Korte, K. F., Ruiken, C. J., Qin, J.-J., Oo, H. & Wessels, L. P. (2008) Membrane fouling and process performance of forward osmosis membranes on activated sludge, *Journal of Membrane Science*, **319** (1–2), 158–168. https://doi.org/10.1016/j.memsci.2008.03.048.

Damirchi, M. & Koyuncu, I. (2021) Nutrient recovery from concentrated municipal wastewater by forward osmosis membrane and $MgCl_2$ based draw solution, *Desalination and Water Treatment*, **211**, 448–455. https://doi.org/10.5004/dwt.2021.26788.

Escobar, I. C. (2010) A summary of challenges still facing desalination and water reuse, *Sustainability Science and Engineering*, **2**, 389–397. https://doi.org/10.1016/S1871-2711(09)00214-1.

Eyvaz, M., Aslan, T., Arslan, S., Yüksel, E. & Koyuncu, I. (2016) Recent developments in forward osmosis membrane bioreactors: A comprehensive review, *Desalination and Water Treatment*, **57** (59), 28610–28645. https://doi.org/10.1080/19443994.2016.1193448.

Gray, G. T., McCutcheon, J. R. & Elimelech, M. (2006) Internal concentration polarization in forward osmosis: Role of membrane orientation, *Desalination*, **197** (1–3), 1–8. https://doi.org/10.1016/j.desal.2006.02.003.

Guo, H., Qin, Q., Hu, M., Chang, J.-S. & Lee, D.-J. (2024) Treatment of refinery wastewater: Current status and prospects, *Journal of Environmental Chemical Engineering*, **12** (2), 112508. https://doi.org/10.1016/j.jece.2024.112508.

Han, J., Dai, P., Gu, C., Liao, Y., Zhao, Y., Razaqpur, A. G., Sun, G. & Chou, S. (2023) Emulsified oily wastewater treatment via fertilizer drawn forward osmosis using a corrugated thin film composite membrane, *Journal of Membrane Science*, **685**, 121926. https://doi.org/10.1016/j.memsci.2023.121926.

Holloway, R. W., Childress, A. E., Dennett, K. E. & Cath, T. Y. (2007) Forward osmosis for concentration of anaerobic digester centrate, *Water Research*, **41** (17), 4005–4014. https://doi.org/10.1016/j.watres.2007.05.054.

Im, S.-J., Jeong, S. & Jang, A. (2021) Forward osmosis (FO)-reverse osmosis (RO) hybrid process incorporated with hollow fiber FO, *npj Clean Water*, **4**, 51. https://doi.org/10.1038/s41545-021-00143-0.

Iorhemen, O. T., Hamza, R. A. & Tay, J. H. (2016) Membrane bioreactor (MBR) technology for wastewater treatment and reclamation: Membrane fouling, *Membranes*, **6** (2), 33. https://doi.org/10.3390/membranes6020033.

Johnson, D., Hashaikeh, R., Hilal, N., (2021) Basic principles of osmosis and osmotic pressure. In: Hilal, N., Ismail, A., Mohamed Khayet, M. & Johnson, D. (eds) *Osmosis Engineering*, Netherlands: Elsevier, pp. 1–15. https://doi.org/10.1016/B978-0-12-821016-1.00011-5.

Kadhima, R. M., Al-Abodi, E. E. & Al-Alawy, A. F. (2018) Citrate-coated magnetite nanoparticles as osmotic agent in a forward osmosis process, *Desalination and Water Treatment*, **115**, 45–52. http://dx.doi.org/10.5004/dwt.2018.22456.

Kessler, J. O. & Moody, C. D. (1976) Drinking-water from sea water by forward osmosis, *Desalination*, **18** (3), 297–306. https://doi.org/10.1016/S0011-9164(00)84119-3.

Kharraz, J. A., Khanzada, N. K., Farid, M. U., Kim, J., Jeong, S. & An, A. K. (2022) Membrane distillation bioreactor (MDBR) for wastewater treatment, water reuse, and resource recovery: A review, *Journal of Water Process Engineering*, **47**, 102687. https://doi.org/10.1016/j.jwpe.2022.102687.

Khudair, W. N. (2011) *Concentration Poisonous Metallic Radicals From Industrial Water by Forward and/or Reverse Osmosis*. MSc Thesis, University of Baghdad, Iraq.

Lee, K. L., Baker, R. W. & Lonsdale, H. K. (1981) Membranes for power generation by pressure-retarded osmosis, *Journal of Membrane Science*, **8** (2), 141–171. https://doi.org/10.1016/S0376-7388(00)82088-8.

Liu, C., Gao, R., Zhang, X., Tong, T., He, Q. & Ma, J. (2024) Controlled architecture of multi-defense anti-fouling forward osmosis membrane for efficient shale gas wastewater treatment, *Journal of Membrane Science*, **699**, 122625. https://doi.org/10.1016/j.memsci.2024.122625.

Loeb, S., Titelman, L., Korngold, E. & Freiman, J. (1997) Effect of porous support fabric on osmosis through a Loeb–Sourirajan type asymmetric membrane, *Journal of Membrane Science*, **129** (2), 243–249. https://doi.org/10.1016/S0376-7388(96)00354-7.

Ma, J., Wang, Z. & Xu, Y., Wang, Q., Wu, Z. & Grasmick, A. (2013) Organic matter recovery from municipal wastewater by using dynamic membrane separation process, *Chemical Engineering Journal*, **219**, 190–199. https://doi.org/10.1016/j.cej.2012.12.085.

Majid, O. A., Hreiz, R., Castel, C. & Favre, E. (2023) Impact of concentration polarization on membrane gas separation processes: From 1D modelling to detailed CFD simulations, *Chemical Engineering Science*, **281**, 119128. https://doi.org/10.1016/j.ces.2023.119128.

Mamah, S. C., Goh, P. S. & Ismail, A. F., Yogarathinam, L. T., Suzaimi, N. D., Opia, A. C., Ojo, S. & Ngwana, N. O. (2022) Bio-polymer modified nanoclay embedded forward osmosis membranes with enhanced desalination performance, *Journal of Applied Polymer Science*, **139** (27), e52473. https://doi.org/10.1002/app.52473.

McCutcheon, J. R. & Elimelech, M. (2006) Influence of concentrative and dilutive internal concentration polarization on flux behavior in forward osmosis, *Journal of Membrane Science*, **284** (1–2), 237–247. https://doi.org/10.1016/j.memsci.2006.07.049.

Ozcan, O., Sahinkaya, E. & Uzal, N. (2023) Integration of direct microfiltration and reverse osmosis process for resource recovery from municipal wastewater, *Desalination and Water Treatment*, **303**, 1–10. https://doi.org/10.5004/dwt.2023.29787.

Qasem, N. A. A., Generous, M. M., Qureshi, B. A. & Zubair, S. M. (2023) Osmotic coefficient. In: Qasem, N., Generous, M., Qureshi, B. & Zubair, S. (eds) *Thermodynamic and Thermophysical Properties of Saline Water*. Cham, Switzerland: Springer, pp. 257–263. https://doi.org/10.1007/978-3-031-35193-8_12.

Salamanca, M., Peña, M., Hernandez, A., Prádanos, P. & Palacio, L. (2023) Forward osmosis application for the removal of emerging contaminants from municipal wastewater: A review, *Membranes*, **13** (7), 655. https://doi.org/10.3390/membranes13070655.

Salih, M. H. & Al-Alawy, A. F. (2022a) $MgCl_2$ and $MgSO_4$ as draw agents in forward osmosis process for East Baghdad oilfield produced water treatment, *Desalination and Water Treatment*, **256**, 80–88. http://dx.doi.org/10.5004/dwt.2022.28408.

Salih, M. H. & Al-Alawy, A. F. (2022b) A novel forward osmosis for treatment of high-salinity east Baghdad oilfield produced water as a part of a zero liquid discharge system, *Desalination and Water Treatment*, **248**, 18–27. https://doi.org/10.5004/dwt.2022.28070.

Schneider, C., Oñoro, A. E., Hélix-Nielsen, C. & Fotidis, I. A. (2021) Forward-osmosis anaerobic-membrane bioreactors for brewery wastewater remediation, *Separation and Purification Technology*, **257**, 117786. https://doi.org/10.1016/j.seppur.2020.117786.

Takabi, A., Shakeri, A. & Razavi, R. (2024) Forward osmosis membrane substrates with low structure parameter: Modification with PSf-g-PMMA graft copolymer, *Journal of Applied Polymer Science*, **141** (35), e55883. https://doi.org/10.1002/app.55883.

Tan, C. H. & Ng, H. Y. (2008) Modified models to predict flux behavior in forward osmosis in consideration of external and internal concentration polarizations, *Journal of Membrane Science*, **324** (1–2), 209–219. https://doi.org/10.1016/j.memsci.2008.07.020.

Tan, C. H. & Ng, H. Y. (2013) Revised external and internal concentration polarization models to improve flux prediction in forward osmosis process, *Desalination*, **309**, 125–140. https://doi.org/10.1016/j.desal.2012.09.022.

Tang, C. Y., She, Q., Lay, W. C. L., Wang, R. & Fane, A. G. (2010) Coupled effects of internal concentration polarization and fouling on flux behavior of forward osmosis membranes during humic acid filtration, *Journal of Membrane Science*, **354** (1–2), 123–133. https://doi.org/10.1016/j.memsci.2010.02.059.

Tortajada, C. & Biswas, A. K. (2018) Achieving universal access to clean water and sanitation in an era of water scarcity: Strengthening contributions from academia, *Current Opinion in Environmental Sustainability*, **34**, 21–25. https://doi.org/10.1016/j.cosust.2018.08.001.

United Nations. (2023) *The Sustainable Development Goals Report: Special Edition*. https://unstats.un.org/sdgs/report/2023/The-Sustainable-Development-Goals-Report-2023.pdf.

van't Hoff, J. H. (1995) The role of osmotic pressure in the analogy between solutions and gases, *Journal of Membrane Science*, **100** (1), 39–44. https://doi.org/10.1016/0376-7388(94)00232-N.

WWAP. (2024) *Water for Prosperity and Peace, The United Nations World Water Development Report*. https://unesdoc.unesco.org/ark:/48223/pf0000388948.

Zhao, S., Zou, L., Tang, C. Y. & Mulcahy, D. (2012) Recent developments in forward osmosis: Opportunities and challenges, *Journal of Membrane Science*, **396**, 1–21. https://doi.org/10.1016/j.memsci.2011.12.023.

First received 13 August 2024; accepted in revised form 6 September 2024. Available online 18 September 2024